An Adaptive Line-of-Sight (ALOS) Guidance Law for Path Following of Aircraft and Marine Craft

Thor I. Fossen, *Fellow, IEEE*

Abstract— This brief presents a novel nonlinear adaptive line-of-sight (ALOS) guidance law for path following, compensating for drift forces due to wind, waves, and ocean currents. The ALOS guidance law is proven to have uniform semiglobal exponential stability (USGES) properties during straight-line path following at constant speed. The ALOS guidance law performs similar to the classical integral line-of-sight (ILOS) and adaptive ILOS guidance laws when the sideslip angle is nearly constant. The ALOS guidance law, however, has better tracking capabilities when compensating for rapidly varying sideslip caused by a time-varying disturbance. This is because the integral state of the ALOS guidance law is additive to the unknown sideslip angle (disturbance matching). In contrast, the ILOS guidance laws must compensate sideslip through a saturating arctangent function. The study also includes an input-to-state stable (ISS) reduced-order extended state observer for estimation of the line-of-sight (LOS) crab angle, known as the ELOS guidance law. The performance of the ALOS, ILOS, and ELOS guidance laws is compared by simulating rapid changes in the sideslip angle to stress the critical assumptions of the algorithms. Finally, a case study of the Remus 100 autonomous underwater vehicle (AUV) exposed to stochastic ocean currents is used to compare the performance of the ILOS, ALOS, and ELOS algorithms during normal operation.

Index Terms— Adaptive control, guidance, land vehicles, marine vehicles, unmanned aerial vehicles (UAVs).

I. Introduction

AIRCRAFT, marine craft, and unmanned vehicles use line-of-sight (LOS) guidance laws to accomplish motion control scenarios, such as object tracking, path following, path tracking, and path maneuvering; see Breivik and Fossen [3], Beard and McLain [1], Fossen [12], Lekkas and Fossen [16], Lin [18], Wilhelm and Clem [31], and Yanushevsky [32] for instance.

Vehicle path-following control systems can be implemented using both heading and course autopilot systems in cascade with a guidance law. This brief studies LOS guidance laws for path following using a *heading autopilot* command ψ_d. The system under consideration is

$$\dot{y}_e^p = U \sin(\psi + \beta_c - \pi_h) \tag{1}$$

$$\psi_d = \pi_h + \theta_2 - \tan^{-1}\left(K_p y_e^p + \theta_1\right) \tag{2}$$

where y_e^p is the cross-track error expressed in a path-tangential reference frame $\{p\}$ rotated an azimuth angle π_h with respect to the North-East reference frame $\{n\}$, ψ is the yaw (heading) angle, $U = (u^2 + v^2)^{1/2}$ is the speed, where (u, v) denotes the surge and sway velocities, and $\beta_c = \tan^{-1}(v/u)$ is the vehicle's crab angle; see Section II for details. It is assumed that the heading autopilot achieves $\psi = \psi_d$, where ψ_d is the LOS yaw angle command (2), which can be tuned by the proportional gain $K_p > 0$. The crab angle β_c is assumed to be unknown, and the control objective is to cancel β_c by using the control signals θ_1 or θ_2 to drive the cross-track error y_e^p to zero. Previous studies assumes that $\theta_1 = \theta_2 = 0$ or that θ_1 can be designed to cancel β_c. The main contribution of this brief is an adaptive law for θ_2, which achieves disturbance matching. The different design techniques and their root in the literature are presented below.

A. LOS Guidance ($\theta_1 = \theta_2 = 0$)

The study in this brief builds on the concept of path following using *proportional guidance* where $K_p = 1/\Delta$, and Δ is the look-ahead distance. The proportional guidance law, $\psi_d = \pi_h - \tan^{-1}(y_e^p/\Delta)$, mimics the heading angle command of an experienced sailor [14]. Applications to marine craft are discussed by Pettersen and Lefeber [26] and Fossen et al. [7]. A similar approach has been applied to small unmanned aerial vehicles (UAVs) by Nelson et al. [23]. This work uses a vector field surrounding the path generating course commands to guide the UAV toward the desired path. A comparative study of the LOS and vector-field guidance laws with application to autonomous underwater vehicles (AUVs) are found by Caharija et al. [5]. Proportional guidance techniques can also be used to guide missiles; see Siouris [29] and Yanushevsky [32]. Model-based predictive control (MPC) has been applied successfully to LOS guidance path following by numerous authors; see Liu et al. [19], Oh and Sun [24], Pavlov et al. [25], and Rout and Subudhi [28].

Uniform global asymptotic stability (UGAS) and uniform local exponential stability (ULES) of the *proportional* LOS guidance law were first proven by Pettersen and Lefeber [26]. This is also referred to as *global κ-exponential stability* as defined by Sørdalen and Egeland [30]. More recently, Fossen and Pettersen [11] have shown that the *proportional* guidance law, when applied to course and heading control, is uniformly semiglobally exponentially stable (USGES). This guarantees strong convergence and robustness properties to perturbations; see Pettersen [27]. An immediate consequence of Fossen and Pettersen [11] is that global exponential stability (GES) of

the proportional LOS guidance law cannot be achieved due to a saturating sinusoidal function in the cross-track error dynamics.

B. ILOS Guidance ($\theta_1 \neq 0$, $\theta_2 = 0$)

Despite the effectiveness and popularity of *proportional* LOS guidance laws, they have limitations when the vehicle is exposed to *drift forces* caused by wind, waves, and ocean currents. In addition, underactuated vehicles cannot produce a sway force. Hence, convergence to the desired path under the influence of drift is a nontrivial task. The consequence can be large cross-track errors during path following. The standard solution to this problem has been to add an integral state θ_1 to the guidance law in an ad hoc manner and rely on linear superposition. This is referred to as *proportional-integral* (PI) guidance. Unfortunately, the PI guidance laws can be challenging to tune, and no global stability results exist.

In 2008, a nonlinear integral LOS (ILOS) guidance law was proposed by Børhaug et al. [2]. In this work, global κ-exponential stable for straight-line path following at constant speed was proven using the Lyapunov stability analysis. Extensions to path following for curved paths using monotone cubic Hermite splines were made by Lekkas and Fossen [17]. The ILOS guidance law has been successfully implemented in many applications, and excellent performance has been demonstrated by Caharija [4] and Caharija et al. [6].

An adaptive ILOS guidance law replacing the integral state with a parameter for sideslip compensation has been proposed by Fossen et al. [10], while Fossen and Lekkas [9] present indirect and direct adaptive control methods for LOS path following. Alternative methods using observer theory have been proposed by Liu et al. [20], [21].

C. ALOS Guidance ($\theta_1 = 0$, $\theta_2 \neq 0$)

The brief's main contribution is a novel adaptive LOS guidance law with USGES stability properties. An adaptive LOS (ALOS) guidance law is proven to have USGES properties during straight-line path following at constant speed. Unknown disturbances due to wind, waves, and ocean currents are modeled as drift, and the ALOS guidance law compensates for this by parameter adaptation. The main difference between the classical and adaptive ILOS guidance laws to the ALOS guidance law is that the integral state θ_1 is replaced by θ_2, which is additive to the unknown crab angle. In contrast, the ILOS guidance law must compensate the crab angle through a saturating arctangent function using the integral state θ_1. The guidance laws have similar tracking performance during normal operations. However, the ALOS guidance law has better tracking capability for rapidly varying crab angles caused by environmental disturbances.

D. Organization of This Brief

Section II contains the kinematic preliminaries, including the cross-track error dynamics expressed in a path-tangential reference frame. Sections III and IV present the classical and adaptive ILOS guidance laws represented by the control signal
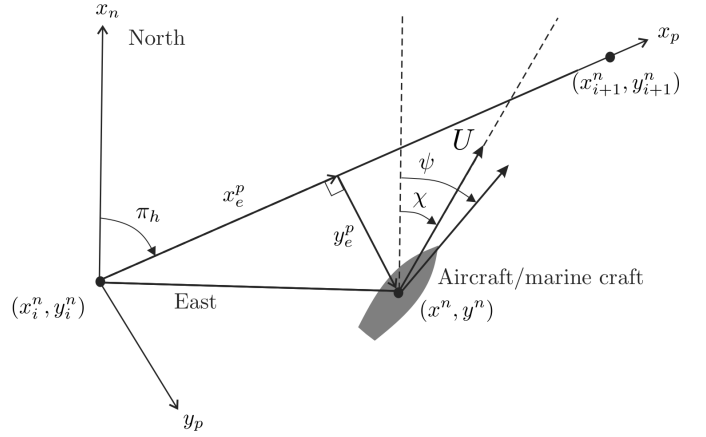

Fig. 1. North-East and path-tangential coordinate systems $\{n\}$ and $\{p\}$, respectively. The along- and cross-track errors are denoted by (x_e^p, y_e^p).

θ_1. Section V discusses the new ALOS guidance law defined by the control signal θ_2, while the extended state observer for LOS path following is presented in Section VI. A comparative study of the guidance laws is presented in Section VII, and Section VIII is a case study based on a high-fidelity model of the Remus 100 AUV. Finally, Section IX concludes the results.

II. KINEMATIC PRELIMINARIES

This section presents the coordinate frames, tracking error dynamics, and kinematic differential equations.

A. Coordinate Systems

For marine craft and aircraft, the six different motion components in the body frame $\{b\}$ are defined as *surge, sway, heave, roll, pitch*, and *yaw*. The North-East coordinate system is denoted by $\{n\}$. Consider a straight-line segment given by two waypoints (x_i^n, y_i^n) and (x_{i+1}^n, y_{i+1}^n) expressed in $\{n\}$ where $i = 1, 2, \ldots, N$. Assume that the path-tangential coordinate system $\{p\}$ has its origin located at (x_i^n, y_i^n), and the x_p-axis is pointing toward the next waypoint (x_{i+1}^n, y_{i+1}^n). Hence, the path-tangential coordinate system can be obtained by rotating the North-East coordinate system $\{n\}$ an angle π_h about the downward z_n-axis, as shown in Fig. 1.

B. Tracking Errors

The *along-* and *cross-track errors* (x_e^p, y_e^p) expressed in $\{p\}$ are given by

$$\begin{bmatrix} x_e^p \\ y_e^p \end{bmatrix} = \boldsymbol{R}_{z,\pi_h}^\top \left(\begin{bmatrix} x^n \\ y^n \end{bmatrix} - \begin{bmatrix} x_i^n \\ y_i^n \end{bmatrix} \right) \tag{3}$$

where (x^n, y^n) is the vehicle's North-East position

$$\boldsymbol{R}_{z,\pi_h} = \begin{bmatrix} \cos(\pi_h) & -\sin(\pi_h) \\ \sin(\pi_h) & \cos(\pi_h) \end{bmatrix} \in \mathrm{SO}(2) \tag{4}$$

and $\pi_h = \mathrm{atan2}(y_{i+1}^n - y_i^n, x_{i+1}^n - x_i^n)$. This can be extended to path following for curved paths using the approach of Fossen and Pettersen [11].

C. Kinematic Differential Equations

Let $\boldsymbol{p}^n = [x^n, y^n]^\top$ be the position vector expressed in $\{n\}$, and $\boldsymbol{v}^b = [u, v]^\top$ be the velocity vector expressed in $\{b\}$. Then, it follows that [12]:

$$\dot{x}^n = u\cos(\psi) - v\sin(\psi) \tag{5}$$

$$\dot{y}^n = u\sin(\psi) + v\cos(\psi) \tag{6}$$

where ψ is the yaw angle.

D. Amplitude-Phase Representation

It is advantageous to express the kinematic differential equations (5) and (6) in amplitude-phase form

$$\dot{x}^n = U\cos(\psi + \beta_c) \tag{7}$$

$$\dot{y}^n = U\sin(\psi + \beta_c) \tag{8}$$

where the amplitude U is the speed over ground (SOG), and β_c is the crab angle given by

$$U = \sqrt{u^2 + v^2} \tag{9}$$

$$\beta_c = \tan^{-1}\left(\frac{v}{u}\right). \tag{10}$$

The course over ground (COG) is recognized as $\chi := \psi + \beta_c$.

E. Influence of Wind, Waves, and Ocean Currents

Aircraft operates in the wind, while marine craft can be exposed to ocean currents, waves, and wind. The aerodynamic and hydrodynamic forces are the functions of the relative velocity vector $\boldsymbol{v}_r^b = \boldsymbol{v}^b - \boldsymbol{v}_f^b$, where $\boldsymbol{v}_f^b = [u_f, v_f]^\top$ is the *flow velocity* vector due to wind, waves, and currents expressed in $\{b\}$. This implies that lift will be perpendicular and drag will be parallel to the relative flow. The linear relative velocities can be expressed by Fossen [12]

$$u_r = U_r\cos(\beta) \tag{11}$$

$$v_r = U_r\sin(\beta) \tag{12}$$

where $U_r = (u_r^2 + v_r^2)^{1/2}$ is the relative speed and

$$\beta = \tan^{-1}\left(\frac{v_r}{u_r}\right) \tag{13}$$

is the *sideslip angle*. Note that the *crab angle*[1] defined by (10) is equal to the sideslip angle when $u_f = v_f = 0$. We can express the crab angle as a function of the flow velocities by

$$\beta_c = \tan^{-1}\left(\frac{v_r + v_f}{u_r + u_f}\right) = \tan^{-1}\left(\frac{\tan(\beta) + \frac{v_f}{U_r\cos(\beta)}}{1 + \frac{u_f}{U_r\cos(\beta)}}\right). \tag{14}$$

This formula is used in Section VI when simulating vehicles exposed to environmental disturbances.

F. Tracking-Error Differential Equations

The tracking-error dynamics expressed in $\{p\}$ is found by time differentiation of (3) and substitution of (7) and (8). This gives the formulas

$$\dot{x}_e^p = U\cos(\psi + \beta_c - \pi_h) \tag{15}$$

$$\dot{y}_e^p = U\sin(\psi + \beta_c - \pi_h). \tag{16}$$

[1] In the literature, the term sideslip angle is often used for the crab angle while we explicitly distinguish between the angles.

III. CLASSICAL ILOS GUIDANCE LAW

The control objective is to choose the yaw angle ψ in (16), such that the cross-track error $y_e^p \to 0$. The LOS algorithms for path following are usually employed at a kinematic level under the assumption that the heading autopilot guarantees that $\psi = \psi_d$. The classical ILOS' guidance law (Børhaug et al. [2]) assumes that β_c is unknown for a given azimuth angle π_h. Hence

$$\psi_d = \pi_h - \tan^{-1}\left(K_{p_y}(y_e^p + \kappa y_{int}^p)\right) \tag{17}$$

$$\dot{y}_{int}^p = \frac{\Delta}{\Delta^2 + \left(y_e^p + \kappa y_{int}^p\right)^2}\, y_e^p \tag{18}$$

where y_{int}^p is the integral state used to compensate β_c as defined by (14), $\Delta > 0$ is the user-specified look-ahead distance, and $K_{p_y} = 1/\Delta$. The integral gain $\kappa > 0$ is a tunable parameter. Substitution of (17) into (16) gives

$$\dot{y}_e^p = U\sin(\beta_c - \tan^{-1}(K_{p_y}(y_e^p + \kappa y_{int}^p))). \tag{19}$$

Hence, β_c must be compensated for by the integral state y_{int}^p to satisfy the control objective. In the stability analysis, the following assumptions will be made.

Assumption 1: The vehicle is moving at positive forward speed $0 < U^{\min} \le U \le U^{\max}$.

Assumption 2: The crab angle β_c is constant during path following, such that $\dot{\beta}_c = 0$.

Assumption 3: The crab angle estimation error $\tilde{\beta}_c = \beta_c - \hat{\beta}_c$, where $\hat{\beta}_c$ is the parameter estimate, is small during path following. When applying integral control instead of parameter adaption, $\hat{\beta}_c \equiv 0$, and thus, $\tilde{\beta}_c = \beta_c$ is small.

Remark 1: Vehicle control systems are designed to keep the relative speed U_r constant and the sideslip angle β small. Because of (14), the crab angle β_c will be nearly constant for a vehicle traversing straight lines and circular paths if the flow velocity vector is nearly constant. Also note the sway velocity v (and, thus, the yaw rate r) will be small during straight-line path following. Straight lines and circles are the main segments used to construct *Dubins paths* [13]. The switching between the segments will appear as steps in the integral state. For vehicles traversing a noncircular feasible path, i.e., a small curvature path, β_c will vary slowly. However, the dynamics of β_c will be much slower than the control bandwidth; thus, integral control will track the changes. Also, note that although the crab angle is relatively small, it primarily affects the path-following properties of the vehicle. Not adequately compensated, this results in significant deviations from the desired path.

For the ILOS guidance law (17) and (18), $\tilde{\beta}_c = \beta_c$ is small by Assumption 3. Hence, $\sin(\beta_c) \approx \beta_c$ and $\cos(\beta_c) \approx 1$. Furthermore, application of the trigonometry identity, $\sin(a - b) = \sin(a)\cos(b) - \cos(a)\sin(b)$, to (19) gives

$$\dot{y}_e^p = U\cos(\tan^{-1}((y_e^p + \kappa y_{int}^p)/\Delta)\beta_c \\ - U\sin(\tan^{-1}((y_e^p + \kappa y_{int}^p)/\Delta). \tag{20}$$

Using $\cos(\tan^{-1}((x + a)/d)) = d/(d^2 + (x + a)^2)^{1/2}$ and $\sin(\tan^{-1}((x + a)/d)) = (x + a)/(d^2 + (x + a)^2)^{1/2}$, the

expression for (20) is further simplified, such that

$$\dot{y}_e^p = -\frac{U(y_e^p + \kappa y_{int}^p)}{\sqrt{\Delta^2 + (y_e^p + \kappa y_{int}^p)^2}} + d \qquad (21)$$

where d is an additive disturbance defined by

$$d := \frac{U\Delta}{\sqrt{\Delta^2 + (y_e^p + \kappa y_{int}^p)^2}}\beta_c \leq d^{\max}. \qquad (22)$$

Assumption 4: The additive disturbance d is nearly constant and upper bounded, so integral action can be applied.

Theorem 1: The classical ILOS guidance law (17) and (18) applied to the cross-track error (16) renders the origin $(y_e^p, y_{int}^p) = (0, \bar{y}_{int}^p)$ USGES under Assumptions 1–4 if the heading autopilot guarantees that $\psi = \psi_d$ and $\kappa \leq \kappa^{\max}$, where the upper bound $\kappa^{\max}$ is defined by Børhaug et al. [2].

Proof: The origin $(y_e^p, y_{int}^p) = (0, \bar{y}_{int}^p)$ is UGAS/ULES as shown by Børhaug et al. [2]. This can be extended to USGES following the approach of Fossen and Pettersen [11].

IV. ADAPTIVE ILOS GUIDANCE LAW

Assumption 4 stating that d given by (22) must be constant can be removed. The adaptive ILOS guidance law of Fossen et al. [10] replaces the integral state (18) with a parameter estimate $\hat{\beta}_c$ according to

$$\psi_d = \pi_h - \tan^{-1}\left(\frac{y_e^p}{\Delta} + \hat{\beta}_c\right) \qquad (23)$$

$$\dot{\hat{\beta}}_c = \gamma \frac{U\Delta}{\sqrt{\Delta^2 + (y_e^p + \Delta\hat{\beta}_c)^2}} y_e^p. \qquad (24)$$

Theorem 2: The adaptive ILOS guidance law (23) and (24) applied to system (16) renders the origin $(y_e^p, \tilde{\beta}_c) = (0, 0)$ USGES under Assumptions 1–3 if $\gamma > 0$, and the heading autopilot guarantees that $\psi = \psi_d$.

Proof: See Fossen et al. [10].

V. ADAPTIVE LOS

The main result of this brief is the ALOS guidance law

$$\psi_d = \pi_h - \hat{\beta}_c - \tan^{-1}\left(\frac{y_e^p}{\Delta}\right) \qquad (25)$$

$$\dot{\hat{\beta}}_c = \gamma \frac{\Delta}{\sqrt{\Delta^2 + (y_e^p)^2}} y_e^p \qquad (26)$$

where γ is the adaptation gain, and $\hat{\beta}_c$ is the parameter estimate. Note that $\hat{\beta}_c$ in (25) is additive to the unknown crab angle in (16). This is referred to as disturbance matching. In contrast, the classical and adaptive ILOS guidance laws must compensate for the crab angle through a saturating arctangent function. Also note that the parameter update law (26) does not include the additional term $\Delta\hat{\beta}_c$ of the adaptive ILOS parameter update law (24) nor the speed U.

Substituting (25) into (16) under the assumption that the heading autopilot guarantees that $\psi = \psi_d$ gives

$$\dot{y}_e^p = U \sin\left(\tilde{\beta}_c - \tan^{-1}\left(\frac{y_e^p}{\Delta}\right)\right) \qquad (27)$$

TABLE I
KEY PROPERTIES AND ASSUMPTIONS OF THE LOS ALGORITHMS

Algorithm	Crab angle	Peaking	Stability
ELOS	Time varying	No peaking	ISS
Classical ILOS	Constant	-	USGES
Adaptive ILOS	Constant	May suffer from peaking	USGES
ALOS	Constant	-	USGES

where $\tilde{\beta}_c = \beta_c - \hat{\beta}_c$. Assumption 2 implies that $\dot{\tilde{\beta}}_c = -\dot{\hat{\beta}}_c$, and application of Assumption 3 to (27) gives the error dynamics

$$\dot{y}_e^p = -\frac{U}{\sqrt{\Delta^2 + (y_e^p)^2}} y_e^p + \frac{U\Delta}{\sqrt{\Delta^2 + (y_e^p)^2}}\tilde{\beta}_c \qquad (28)$$

$$\dot{\tilde{\beta}}_c = -\gamma \frac{\Delta}{\sqrt{\Delta^2 + (y_e^p)^2}} y_e^p. \qquad (29)$$

Theorem 3: The ALOS guidance law (25) and (26) applied to the system (16) renders the origin $(y_e^p, \tilde{\beta}) = (0, 0)$ USGES under Assumptions 1–3 if the heading autopilot guarantees that $\psi = \psi_d$ and $\gamma > 0$.

Proof: See Appendix A.

VI. EXTENDED STATE OBSERVER FOR LOS PATH FOLLOWING

Liu et al. [21] have derived a reduced-order extended state observer (ESO) for estimation of the crab angle, given by

$$\hat{\beta}_c = \frac{\hat{g}}{U \cos(\psi - \pi_h)} \qquad (30)$$

with

$$\dot{p} = -kp - k^2 y_e^p - kU \sin(\psi - \pi_h) \qquad (31)$$

$$\hat{g} = p + k y_e^p \qquad (32)$$

where $k > 0$ and $p(0) = -k y_e^p(0)$. The estimation error $\tilde{g} = g - \hat{g}$ satisfies the differential equation $\dot{\tilde{g}} = -k\tilde{g} - \dot{g}$. Liu et al. [21] have derived conditions for the state $\tilde{g}$ to be input-to-state stable (ISS) with the input being $\dot{g}$. The ESO-based LOS (ELOS) guidance law is chosen as (23). The observer (30)–(32) is capable of estimating a time-varying crab angle β_c.

VII. COMPARATIVE STUDY OF THE GUIDANCE LAWS

The goal of the case study is to stress test the critical assumptions of the guidance laws by computer simulations. The following algorithms are tested.

ELOS [21]:

$$\dot{p} = -kp - k^2 y_e^p - kU \sin(\psi - \pi_h) \qquad (33)$$

$$\hat{\beta}_c = \frac{p + k y_e^p}{U \cos(\psi - \pi_h)} \qquad (34)$$

$$\psi_d = \pi_h - \tan^{-1}\left(\frac{y_e^p}{\Delta} + \hat{\beta}_c\right). \qquad (35)$$

Classical ILOS [2]:

$$\psi_d = \pi_h - \tan^{-1}\left(\frac{y_e^p + \kappa y_{int}^p}{\Delta}\right) \qquad (36)$$

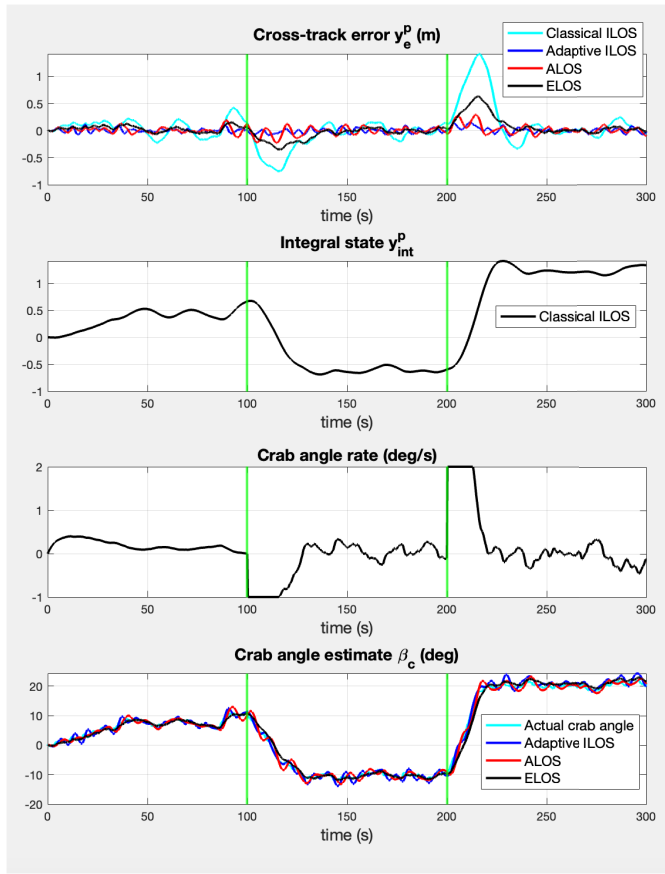$$\dot{y}_{int}^p = \frac{\Delta}{\Delta^2 + (y_e^p + \kappa y_{int}^p)^2} y_e^p. \qquad (37)$$

Fig. 2. Performance of the classical ILOS, adaptive ILOS, ALOS, and ELOS algorithms when β_c (deg) is allowed to vary as a function of time. The green vertical lines separate Phases 1–3.

Fig. 3. Remus 100 AUV at the AUR Laboratory at the Norwegian University of Science and Technology, Trondheim, Norway. URL: https://www.ntnu.edu/aur-lab/auv-remus-100.

Phase 1 (0 ≤ t < 100): Initial phase showing the convergence of the integral state and crab angle estimates when the crab angle is increased slowly from 0 to 10.0 deg. The maximum crab angle rate is $|\dot{\beta}_c| \leq 0.4$ deg/s.

Phase 2 (100 ≤ t < 200): The crab angle is decreased from 10.0 to −20.0 deg, and $|\dot{\beta}_c| \leq 1.0$ deg/s.

Phase 3 (200 ≤ t < 300): The crab angle is increased from −20.0 to 20.0 deg, and $|\dot{\beta}_c| \leq 2.0$ deg/s.

Fig. 2 shows the exponential convergence of y_e^p to zero during Phases 1–3 for the four guidance laws when the vehicle is exposed to stochastic disturbances. The classical ILOS algorithm shows a performance reduction compared with the other guidance laws during Phases 2 and 3 when the crab angle is allowed to vary rapidly. During these phases, $|\dot{\beta}_c|$ is 1.0–2.0 deg/s. The adaptive ILOS and ALOS algorithms, and the ELOS algorithm keep the cross-track error y_e^p close to zero even when β_c is time-varying. As shown by Liu et al. [20], the adaptive guidance laws may suffer from peaking and oscillation behaviors during the transient state, since a large initial tracking error may deteriorate the learning process. The largest oscillations are observed for the adaptive ILOS algorithm, but there are also some oscillations in the ALOS algorithm, particularly when $|\dot{\beta}_c|$ is large. The overall conclusion is that the ALOS and ELOS algorithms outperform the other two when $|\dot{\beta}_c|$ is large. The ELOS algorithm removes the oscillations to the price of degrading the USGES stability property to ISS. However, during normal operation (Phase 1), the performance of the four algorithms is quite similar. The case study also confirms that the ALOS assumption that β_c is constant can be relaxed, since $|\dot{\beta}_c| \leq 2.0$ deg/s gives accurate regulation of the cross-track error to zero.

VIII. CASE STUDY WITH THE REMUS 100 AUV

Since the ALOS guidance law outperforms the adaptive ILOS guidance law, it was decided to compare the ALOS guidance law with the classical ILOS and ELOS guidance laws using a high-fidelity model of the Remus 100 AUV; see Fig. 3. The goal is to evaluate the efficiency and robustness of the AUV during normal operation when the AUV is exposed to a stochastic ocean current.

The three guidance laws were implemented with $\Delta = 10$ m. The ILOS integrator gain was chosen as $\kappa = 0.1$. The ALOS adaptation gain was chosen as $\gamma = 0.0006$, while the ELOS gain was $k = 0.5$. The initial current speed was chosen as $V_c = 1.0$ m/s with direction $\beta_{V_c} = 180.0$ deg (see Fig. 4). The sampling time was selected as 20 Hz.

The mathematical model of the AUV is available in the MATLAB MSS toolbox; see Fossen and Perez [8]. The script remus100.m describes an AUV of length 1.6 m, a cylinder
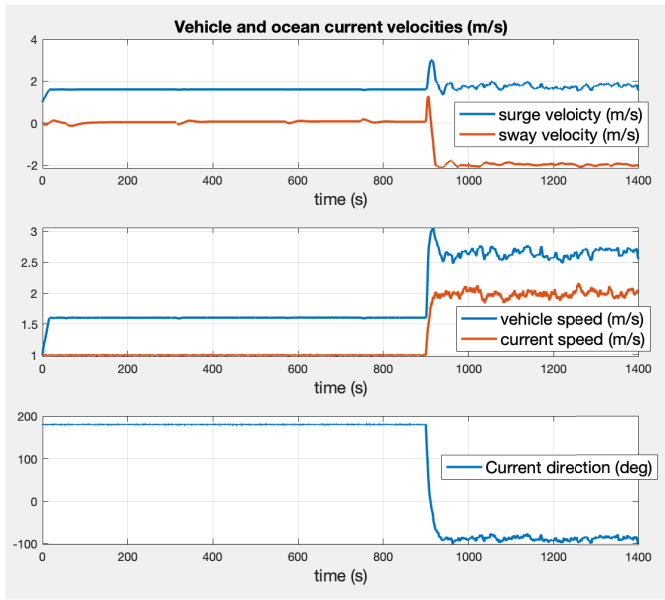
Adaptive ILOS [10]:

$$\psi_d = \pi_h - \tan^{-1}\left(\frac{y_e^p}{\Delta} + \hat{\beta}_c\right) \qquad (38)$$

$$\dot{\hat{\beta}}_c = \gamma \frac{U\Delta}{\sqrt{\Delta^2 + (y_e^p + \Delta\hat{\beta}_c)^2}} y_e^p. \qquad (39)$$

ALOS (main result of Section V):

$$\psi_d = \pi_h - \hat{\beta}_c - \tan^{-1}\left(\frac{y_e^p}{\Delta}\right) \qquad (40)$$

$$\dot{\hat{\beta}}_c = \gamma \frac{\Delta}{\sqrt{\Delta^2 + (y_e^p)^2}} y_e^p. \qquad (41)$$

The properties and assumptions of the different LOS algorithms are summarized in Table I. The guidance laws were implemented using $\Delta = 20.0$ m. The ILOS integrator gain was tuned to obtain maximum performance, and the chosen value was $\kappa = 3.0$. A similar approach was used to find the adaptive ILOS and ALOS adaptation gain $\gamma = 0.2$, while the ELOS observer used $k = 0.5$. The initial states were chosen as $y_e^p(0) = 0$ m, $y_{int}^p(0) = 0$, $\hat{\beta}_c(0) = 0$, and $p(0) = 0$. The sampling time was selected as 20 Hz. It is assumed that the vehicle control system keeps the speed at $U = 2.0$ m/s during path following. Hence, the environmental disturbances can be simulated by perturbing β_c according to (14). Three phases are considered.

Fig. 4. Vehicle speed $U = (u^2 + v^2)^{1/2}$ (m/s), current speed V_c (m/s), and current direction β_{V_c} (deg).
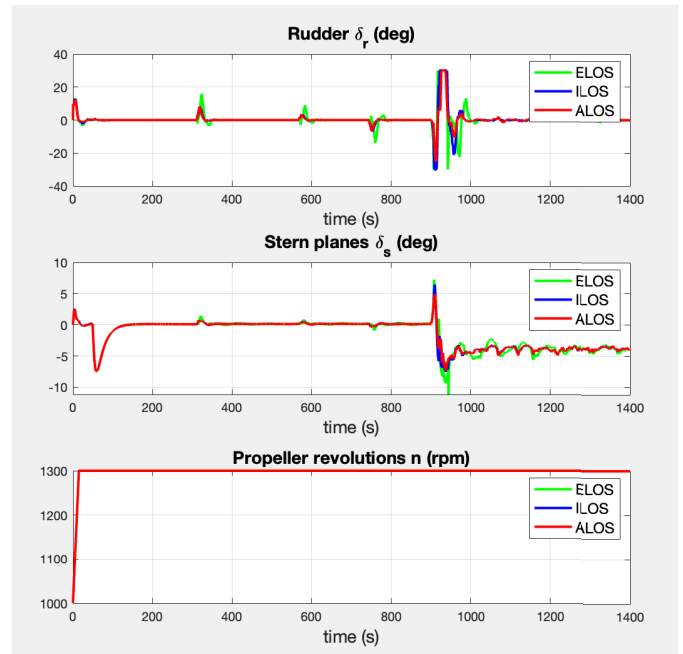

Fig. 5. Commanded rudder angle δ_r (deg), commanded stern-plane angle δ_s (deg), and propeller revolution n (rpm) for the ELOS, ILOS, and ALOS guidance laws.

diameter of 19.0 cm, a mass of 31.9 kg, and a trim weight of 1.0 kg. The vehicle's maximum speed is 2.5 m/s, obtained by running the propeller at 1525 rpm in zero currents. The endurance is 22 h at the optimum speed of 1.5 m/s. Depth is controlled using the stern plane δ_s, and the heading angle is controlled using a tail rudder δ_r. In the case study, the following control systems have been implemented (see Fig. 5).

A. Propeller Revolution

The propeller revolution is increased linearly from 1000 to 1300 rpm (see Fig. 5) until the AUV reaches its cruise speed.

B. Depth

The depth is changed from 0 to 20 m, as shown in Fig. 6, using successive-loop closure

$$\theta_d = K_{p_z}\left((z^n - z_d^n) + \frac{1}{T_z}\int_0^t (z - z_d)d\tau\right) \quad (42)$$

$$\delta_s = -K_{p_\theta}(\theta - \theta_d) - K_{d_\theta}q - K_{i_\theta}\int_0^t (\theta - \theta_d)d\tau \quad (43)$$

where θ_d is the desired pitch angle, z^n is the heave position, θ is the pitch angle, and q is the pitch rate. The controller gains and time constant can be computed using pole placement [1, Sec. 6.4]. However, trial and failure gave excellent performance for $K_{p_z} = 0.1$, $T_z = 100.0$ s, $K_{p_\theta} = 2.0$, $K_{d_\theta} = 3.0$, and $K_{i_\theta} = 0.1$. The maximum allowed stern-plane deflection is chosen as ±30 deg.

C. Heading

The ILOS guidance law (17) and (18) and the ALOS guidance law (25) and (26) are used to compute the desired yaw angle ψ_d during path following; see Fig. 7. The PI

derivative (PID) controller is

$$\delta_r = -K_{p_\psi}\text{ssa}(\psi - \psi_d) - K_{d_\psi}r - K_{i_\psi}\int_0^t \text{ssa}(\psi - \psi_d)d\tau \quad (44)$$

where ψ is the yaw angle and r is the yaw rate. The controller gains are chosen using pole placement [12, Algorithm 15.1]. This gave $K_{p_\psi} = 7.5$, $K_{d_\psi} = 15.0$, and $K_{i_\psi} = 0.75$ corresponding to a natural frequency of 0.18 rad/s and a relative damping ratio of 1.0 in yaw. The maximum rudder angle deflection is ±30.0 deg. The unconstrained yaw angle tracking error $\tilde{\psi} = \psi - \psi_d$ is mapped to the interval $[-\pi, \pi)$ using the operator ssa : $\mathbb{R} \to [-\pi, \pi)$ representing the smallest difference between the two angles ψ and ψ_d. The MATLAB MSS toolbox implementation is ssa.m. The goal is to follow a path given by the following six waypoints:

```
wpt.pos.x = [0, 150, 300, 200, 0,    0   ]
wpt.pos.y = [0, 200, 400, 800, 1000, 1200].
```

A switching mechanism for selecting the next waypoint is used when moving along the piecewise linear path. Waypoint (x_{i+1}^n, y_{i+1}^n) is selected based on whether or not the vehicle lies within a circle of acceptance with radius $R = 10$ m around (x_{i+1}^n, y_{i+1}^n). In other words, if the vehicle's position (x^n, y^n) at time t satisfies

$$\left(x_{i+1}^n - x^n\right)^2 + \left(y_{i+1}^n - y^n\right)^2 \leq R^2 \quad (45)$$

the next waypoint (x_{i+1}^n, y_{i+1}^n) is selected. The case study is as follows.

Phase 1: The Remus 100 AUV starts at an position $(x^n(0), y^n(0)) = (0 \text{ m}, 0 \text{ m})$ and heading $\psi(0) = 0$ deg at time $t = 0$. During the first phase (0–900 s), the vehicle accelerates up to its cruise speed while exposed to a

Fig. 6. Depth z^n (m), roll angle ϕ (deg), pitch angle θ (deg), and yaw angle ψ (deg) for the ELOS, ILOS, and ALOS guidance laws.
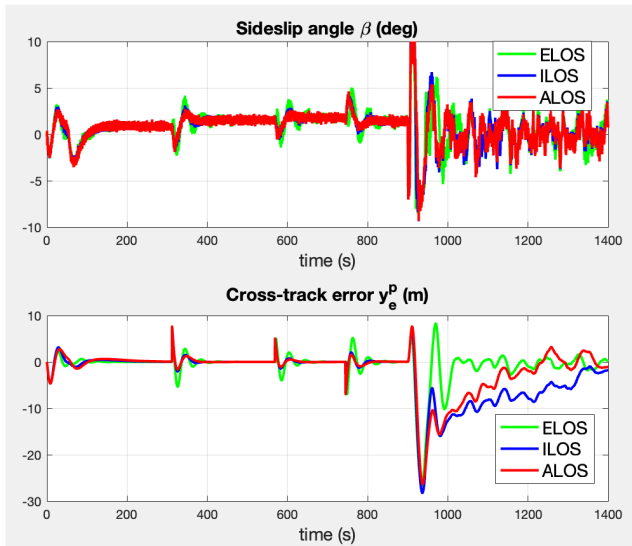

Fig. 7. Sideslip angle β (deg) and cross-track error y_e^p (m) for the ELOS, ILOS, and ALOS guidance laws.

stochastic ocean current with constant magnitude and direction ($V_c = 1.0$ m/s and $\beta_{V_c} = 180.0$ deg). The current increases the vehicle's speed during the first phase, as shown in Fig. 4. The sideslip angle β varies slowly when traversing through the waypoints; see Fig. 7. The performance of the ILOS, ALOS, and ELOS guidance laws is similar, and excellent tracking is obtained for all the algorithms; see Fig. 7.

Phase 2: After 900 s, an extreme stochastic current is simulated. The current's direction β_{V_c} is changed from 180.0 to -180.0 deg in 1 min. At the same time, the magnitude V_c of

the current is increased from 1.0 to 2.0 m/s. The ILOS and ALOS algorithms handle the time-varying current quite well, even though both assume that β_c and U are constant during path following. As expected, the performance of the ELOS algorithm is best in extreme situations with a rapidly varying β_c. It is interesting to notice that the ALOS algorithm has a slightly better tracking performance than the ILOS algorithm when studying the cross-track error y_e^p during rapidly changing current speed and direction (time 900–1400 s). Also note that the ELOS algorithm has larger overshoots than the other algorithms even though the estimate of β_c is smoother.

IX. Conclusion

A novel nonlinear ALOS guidance law for vehicle path following, which compensates for drift forces due to wind, waves, and ocean currents, has been presented. The equilibrium points of the cross-track and parameters estimation errors are shown to be USGES during straight-line path following at constant speed. This guarantees strong convergence and robustness properties to perturbations. Furthermore, it was demonstrated that the ALOS guidance law performs similar to the classical ILOS guidance law by Børhaug et al. [2] when the sideslip angle is nearly constant. The ALOS guidance law, however, has better tracking capabilities when compensating for rapidly varying sideslip caused by a time-varying disturbance. This is because the integral state of the ALOS guidance law is additive to the unknown sideslip angle (disturbance matching). The case study used a high-fidelity model of the Remus 100 AUV exposed to a severe stochastic ocean current. It was concluded that both the ALOS and the classical ILOS guidance laws give excellent performance and robustness for normal AUV operations. In contrast, the ILOS guidance law must compensate sideslip through a saturating arctangent function. The case study also compared the ILOS and ALOS guidance laws with a disturbance observer for β_c, which can handle rapidly varying sideslip. As expected, the observer-based guidance law (ELOS) gave smoother estimates of β_c and better accuracy for large values of the crab angle rate $\dot{\beta}_c$. However, the ILOS and ALOS guidance law had less overshoot than the ELOS algorithm when considering the cross-track error y_e^p.

Future studies should analyze the stability of the feedback interconnection of the ALOS guidance law and the heading autopilot for varying plant parameters and environmental conditions. The assumption that the crab angle is small should be relaxed by extending the stability proofs to arbitrary crab angles.

Appendix

A. Proof of Theorem 3

The error dynamics (28) can be expressed as follows:

$$\dot{x} = \Omega(x)Ax \qquad (46)$$

where $x = [x_1, x_2]^\top := [y_e^p, \tilde{\beta}_c]^\top$ and

$$A = \begin{bmatrix} -U/\Delta & U \\ -\gamma & 0. \end{bmatrix}, \quad \Omega(x) := \frac{\Delta}{\sqrt{\Delta^2 + x_1^2}}. \qquad (47)$$

The characteristic equation, $\det(A - \lambda I_2) = 0$, becomes $\lambda^2 + (U/\Delta)\lambda + \gamma U = 0$. Since $U > 0$ and $\Delta > 0$, the matrix A is *Hurwitz* if the adaptive gain $\gamma > 0$. Consider the nominal system $\dot{x} = \Omega(x)Ax$ and Lyapunov function $W(x) = (1/2)x^\top P x$ with $P = P^\top > 0$. Consequently

$$\dot{W}(x) = \Omega(x)x^\top(PA + A^\top P)x. \tag{48}$$

Let $Q = \text{diag}\{q_1, q_2\} > 0$. Then, P and Q satisfy the Lyapunov equation $PA + A^\top P = -Q$ and

$$\dot{W}(x) = -\Omega(x)x^\top Q x$$
$$< 0 \quad \forall x \neq 0. \tag{49}$$

For each $r > 0$ and all $\|x(t)\| \leq r$, we have that

$$\Omega(x) \geq \frac{\Delta}{\sqrt{\Delta^2 + r^2}} := c(r). \tag{50}$$

Let $p_{\min} = \lambda_{\min}\{P\}$ and $p_{\max} = \lambda_{\max}\{P\}$ be the minimum and maximum eigenvalues of the matrix P, respectively, and $q_{\min} = \min\{q_1, q_2\}$ and $q_{\max} = \max\{q_1, q_2\}$. Consequently

$$\dot{W}(x) \leq -c(r)x^\top Q x \leq -2\frac{q_{\min}}{p_{\max}}c(r)W(x). \tag{51}$$

Since $W(x) > 0$ and $\dot{W}(x) < 0$ whenever $x \neq 0$, it follows from [15, Th. 4.8] that the origin $x = 0$ is uniformly stable and $\|x(t)\| \leq \|x(t_0)\|, \forall t \geq t_0$. The above holds for all trajectories generated by the initial conditions $x(t_0)$. Hence, we can invoke the comparison lemma (see [15, Lemma 3.4]) by noticing that the system $\dot{\chi} = -2(q_{\min}/p_{\max})c(r)\chi$ has the solution $\chi(t) = e^{-2(q_{\min}/p_{\max})c(r)(t-t_0)}\chi(t_0)$, which implies that $\dot{w}(t) \leq e^{-2(q_{\min}/p_{\max})c(r)(t-t_0)}w(t_0)$ for $w(t) = W(x)$. Hence

$$\|x(t)\| \leq \sqrt{\frac{p_{\max}}{p_{\min}}}e^{-\frac{q_{\min}}{p_{\max}}c(r)(t-t_0)}\|x(t_0)\| \tag{52}$$

for all $t \geq t_0$, $\|x(t_0)\| \leq r$ and any $r > 0$. This allows us to conclude that the equilibrium point $x = 0$ of (46) is USGES (see [22, Definition 2.7]).

REFERENCES

[1] R. W. Beard and T. W. McLain, *Small Unmanned Aircraft. Theory and Practice*. Princeton, NJ, USA: Princeton Univ. Press, 2012.

[2] E. Børhaug, A. Pavlov, and K. Y. Pettersen, "Integral LOS control for path following of underactuated marine surface vessels in the presence of constant ocean currents," in *Proc. 47th IEEE Conf. Decis. Control*, Cancun, Mexico, 2008, pp. 4984–4991.

[3] M. Breivik and T. I. Fossen, "Guidance laws for autonomous underwater vehicles," in *Intelligent Underwater Vehicles*, A. V. Inzartsev, Ed. Vienna, Austria: I-Tech Education and Publishing, 2009, pp. 51–76.

[4] W. Caharija, "Integral line-of-sight guidance and control of underactuated marine vehicles," Ph.D. thesis, Dept. Eng. Cybern., Norwegian Univ. Sci. Technol., Trondheim, Norway, 2014.

[5] W. Caharija, K. Y. Pettersen, P. Calado, and J. Braga, "A comparison between the ILOS guidance and the vector field guidance," *IFAC-PapersOnLine*, vol. 48, no. 16, pp. 89–94, 2015.

[6] W. Caharija et al., "Integral line-of-sight guidance and control of underactuated marine vehicles: Theory, simulations, and experiments," *IEEE Trans. Control Syst. Technol.*, vol. 24, no. 5, pp. 1623–1642, Sep. 2016.

[7] T. I. Fossen, M. Breivik, and R. Skjetne, "Line-of-sight path following of underactuated marine craft," *IFAC Proc. Volumes*, vol. 36, no. 21, pp. 211–216, 2003.

[8] T. I. Fossen and T. Perez. (2004). *Marine Systems Simulator (MSS)*. [Online]. Available: https://github.com/cybergalactic/MSS

[9] T. I. Fossen and A. M. Lekkas, "Direct and indirect adaptive integral line-of-sight path-following controllers for marine craft exposed to ocean currents," *Int. J. Adapt. Control*, vol. 31, no. 4, pp. 445–463, Mar. 2017.

[10] T. I. Fossen, K. Y. Pettersen, and R. Galeazzi, "Line-of-sight path following for Dubins paths with adaptive sideslip compensation of drift forces," *IEEE Trans. Control Syst. Technol.*, vol. 23, no. 2, pp. 820–827, Mar. 2015.

[11] T. I. Fossen and K. Y. Pettersen, "On uniform semiglobal exponential stability (USGES) of proportional line-of-sight guidance laws," *Automatica*, vol. 50, no. 11, pp. 2912–2917, Nov. 2014.

[12] T. I. Fossen, *Handbook of Marine Craft Hydrodynamics and Motion Control*, 2nd ed. Hoboken, NJ, USA: Wiley, 2021.

[13] L. Dubins, "On curves of minimal length with a constraint on average curvature, and with prescribed initial and terminal positions and tangents," *Amer. J. Math.*, vol. 79, no. 3, pp. 497–516, 1957.

[14] A. J. Healey and D. Lienard, "Multivariable sliding mode control for autonomous diving and steering of unmanned underwater vehicles," *IEEE J. Ocean. Eng.*, vol. 18, no. 3, pp. 327–339, Jul. 1993.

[15] H. K. Khalil, *Nonlinear Systems*. Upper Saddle River, NJ, USA: Prentice-Hall, 2002.

[16] A. M. Lekkas and T. I. Fossen, "Line-of-sight guidance for path following of marine vehicles," in *Advanced in Marine Robotics*, O. Gal, Ed. Saarbruecken, Germany: LAP LAMBERT Academic Publishing, 2013, pp. 63–92.

[17] A. M. Lekkas and T. I. Fossen, "Integral LOS path following for curved paths based on a monotone cubic Hermite spline parametrization," *IEEE Trans. Control Syst. Technol.*, vol. 22, no. 6, pp. 2287–2301, Nov. 2014.

[18] C. Lin, *Modern Navigation, Guidance, and Control Processing*. Englewood Cliffs, NJ, USA: Prentice-Hall, 1991.

[19] C. Liu, J. Sun, and Z. Zou, "Integrated line of sight and model predictive control for path following and roll motion control using rudder," *J. Ship Res.*, vol. 59, no. 2, pp. 99–112, 2015.

[20] L. Liu, D. Wang, Z. Peng, and H. Wang, "Predictor-based LOS guidance law for path following of underactuated marine surface vehicles with sideslip compensation," *Ocean Eng.*, vol. 124, pp. 340–348, Sep. 2016.

[21] L. Liu, D. Wang, and Z. Peng, "ESO-based line-of-sight guidance law for path following of underactuated marine surface vehicles with exact sideslip compensation," *IEEE J. Ocean. Eng.*, vol. 42, no. 2, pp. 477–487, Apr. 2017.

[22] A. Loria and E. Panteley, "Cascaded nonlinear time-varying systems: Analysis and design," in *Advanced Topics in Control Systems Theory*, F. Lamnabhi-Lagarrigue, A. Loria, and E. Panteley Eds. London, U.K.: Springer-Verlag, 2004, ch. 2, pp. 23–64.

[23] D. R. Nelson, D. B. Barber, T. W. McLain, and R. W. Beard, "Vector field path following for miniature air vehicles," *IEEE Trans. Robot.*, vol. 23, no. 3, pp. 519–529, Jun. 2007.

[24] S.-R. Oh and J. Sun, "Path following of underactuated marine surface vessels using line-of-sight based model predictive control," *Ocean Eng.*, vol. 37, nos. 2–3, pp. 289–295, 2010.

[25] A. Pavlov, H. Nordahl, and M. Breivik, "MPC-based optimal path following for underactuated vessels," *IFAC Proc. Volumes*, vol. 42, no. 18, pp. 340–345, 2009.

[26] K. Y. Pettersen and E. Lefeber, "Way-point tracking control of ships," in *Proc. 40th IEEE Conf. Decis. Control*, Orlando, FL, USA, Dec. 2001, pp. 940–945.

[27] K. Y. Pettersen, "Lyapunov sufficient conditions for uniform semiglobal exponential stability," *Automatica*, vol. 78, pp. 97–102, Apr. 2017.

[28] R. Rout and B. Subudhi, "Design of line-of-sight guidance law and a constrained optimal controller for an autonomous underwater vehicle," *IEEE Trans. Circuits Syst. II, Exp. Briefs*, vol. 68, no. 1, pp. 416–420, Jan. 2021.

[29] G. M. Siouris, *Missile Guidance and Control Systems*. New York, NY, USA: Springer-Verlag, 2010.

[30] O. J. Sørdalen and O. Egeland, "Exponential stabilization of nonholonomic chained systems," *IEEE Trans. Autom. Control*, vol. 40, no. 1, pp. 35–49, Jan. 1995.

[31] J. P. Wilhelm and G. Clem, "Vector field UAV guidance for path following and obstacle avoidance with minimal deviation," *J. Guid., Control, Dyn.*, vol. 42, no. 8, pp. 1848–1856, Aug. 2019.

[32] R. Yanushevsky, *Guidance of Unmanned Aerial Vehicles*. Boca Raton, FL, USA: CRC Press, 2011.